Applied Laser Technology
**Vol. 29, No.1,JAN (2022), pp.01–05**

# ISAR imaging at high resolution in the bistatic radar receiver canted region

Y SIVA PRASAD[1] , G. MALYADRI [2]
Assistant professor[1,2]
DEPARTMENT OF ELECTRICAL AND ELECTRONICS ENGINEERING
P.B.R.VISVODAYA INSTITUTE OF TECHNOLOGY & SCIENCE
S.P.S.R NELLORE DIST, A.P , INDIA , KAVALI-524201

## Abstract

***Research into bistatic radar systems has recently risen to prominence as a means of circumventing the drawbacks of monostatic inverse synthetic aperture radar (ISAR) imaging, which are caused by the system's dependence on a single, stationary antenna. However, for time-varying biostatic angle and equivalent line of sight (LOS) aspect, it is becoming more challenging to obtain a high resolution ISAR image of a manoeuvring target in the receiver-cantered region area of bistatic radar. This work proposes a Radon transform-based super-resolution imaging approach that utilizes a temporal chirp distribution search (TCDS) algorithm. This technique makes an effort to calculate, for high-order phase terms in the cross-range, an approximate chirp rate and its rate of change. Radon-TCDS-Relax is a technique that generates high resolution images by extracting additional target scattering centers after adjusting for high order phase error. To show how well the suggested strategy works, simulation results are presented.***

## Keywords:

***Imaging via Interferometric Scanning with a Reflector less (ISAR) radar, Bistatic radar, Time Chirp distribution Search Radon transform, super resolution, Spread out your scattered centers more.***

## Introduction

High-resolution, long-distance pictures of moving objects obtained using Inverse Synthetic Radar (ISAR) imaging are very valuable for automated target identification and other purposes. In the event of a target moving along the line of sight (LOS), a high resolution ISAR picture is often difficult to be created by a monostatic radar, even when using a sophisticated ISAR imaging algorithm [1-3]. The bistatic radar system has recently been a focus of study [3,4] as a means of overcoming the shortcomings of traditional monostatic radar. The transmitter and receiver in a bistatic ISAR system are located at different locations [5]. This spatial separation makes the radar system more reliable in a number of ways, including the ability to obtain a wider range of useful target information and operate at greater distances and with greater safety on the battlefield. However, the target and radar geometry become more complicated due to the separated transmitter and receiver, and the effect of the separated transmitter and receiver is readily apparent. Therefore, the relationship between the bistatic angle and the azimuth angle of equivalent line of sight (LOS) is a crucial feature of the bistatic ISAR system that needs careful investigation. Biostability in radar has significant effects on both the form and the directional radial wave number. This paper will proceed as described below. Section 2 develops the geometry model of Bistatic ISAR, discusses how the bistatic angle and the azimuth angle of equivalent line of sight (LOS) affect ISAR echoes, and looks into the connection between ISAR

echoes and the time-variable bistatic angle in the receiver-center region. The range eve lope and cross range processing are investigated in depth in Section 3, along with the impact of the changing bistatic angle on ISAR imaging. In Section 4, we offer an approach (Radon-TCDS Relax) that combines the Time Chirp-rate Distribution Search technique with Relax in order to estimate the chirp rate and quadratic chirp rate necessary to remove the high-order phase components caused by the bistatic angle in the two-polar region. In Section 5, we provide simulation results that show how well the suggested strategy works.

## A Model for Bistatic ISAR Signals

## ISAR bistatic geometry

The target is lighted by the transmitter, and the receiver processes the reflected light and other information to create an image, same as in monostatic radar. By broadcasting wideband pulses, Bistatic radar is able to achieve high-range resolution, and by coherently integrating the echoes backscattered from multiple aspects, it is able to attain cross-range resolution, comparable to the monostatic system. However, unlike monostatic radar, bistatic radar has a more complex echoes-from-target propagation [1-5]. Figure 1 depicts the geometry of a bistatic radar

ISSN: 1000-372X ALT

system. Figure 1 depicts the coordinate system and parameters characterizing bistatic radar operating in the x, y plane using a north-referenced two-dimensional coordinate system. The origin point o is located at the baseline's midway L, whereas the transmitter and receiver are situated at Tx(L/2, 0) and Rx(L/2), respectively. Slant range for the transmitter and receiver may be expressed as RR 14 RRRR, RT 14 RT RT, with RT 14 12 cosT ; sinT T and RT 14 12 cosT ; sinT T, respectively. Re = RR + RT = 2 cos [cose, sine] T is equal to the sum of the bisects of the angles RR and RT. Angle between axis x and LOS is e, therefore o" is the monostatic radar equivalent and R'e is the line of sight [1]. The half bistatic angle is defined as e = (R + T)/2, whereas = (R T)/2 is known as the diastatic angle. The bisector unit vector is written as Re 14 cose; sine 12 T, whereas the target's unit vector, v, is written as v = v [cos v, sin v] T. With knowledge of three of the parameters R, T, L, and R, the remaining can be determined using eq. (25) from the literature [1]. Changes in may lead to shifts in backing.

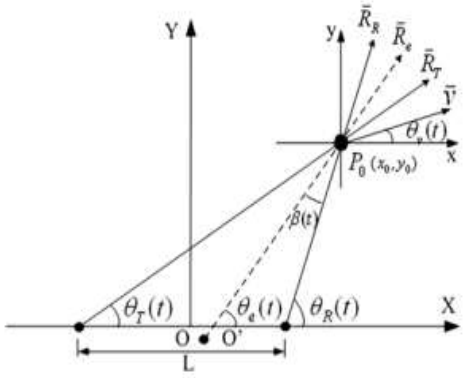


***figure 1 Geometry of Bistatic ISAR model.***

region, which has effect on the range resolution. Similarly, the varied θe of each of echoes has effect on the cross-range resolution. Therefore, the parameters βm and θem are the two key parameters whose values and variations have significantly affect on the characteristic of echoes.

## Effect on the envelope and phase from bistatic angle in receiver cantered region

When the medium resolution involved, the variation of bistatic angle can be ignored for uniformed motion target, therefore we have Ωβ = 0 and get RnΩ(tm)=(xn − ynΩe · tm) · cos β0, in which case an FFT-based approach may be sufficient to generate the ISAR image of target. While when high resolution images are required, it isnecessary to study the effect of the ISAR image when biostatics angle Ωβ ≠ 0. The faster motion target moving and shorter distance of target to receiver radar, the more complexity in bistatic ISAR imaging become. Typically, migration resolution cell phenomenon is the prominent problem to be concerned. Because of the great variation of biostatics angle β and equivalent LOS θem, therefore MTRC phenomenon cannot be ignored. After compensating for the translational motion, the signal in the spatial frequency domain can be expressed as

$$s(f,t_m)=\sum_n A_n \exp[-j\frac{4\pi}{c}(f_c+f_r)R_{n\Omega}(t_m)]$$

where f ∈ [−B/2, B/2]. Ignoring the term higher than the third order, we have

ISSN: 1000-372X ALT

$$R_{n\Omega}(t_m) = R_\Omega + R'_\Omega t_m + R''_\Omega t_m^2 + R'''_\Omega t_m^3$$

where

$$R_\Omega = x_n \cos\beta_0$$

$$R'_\Omega = -\left(y_n \cos\beta_0 \Omega_e + x_n \sin\beta_0 \Omega_\beta\right)$$

$$R''_\Omega = \left\{ \left[ \frac{1}{2} x_n \left( \Omega_e^2 + \Omega_\beta^2 \right) - y_n \dot{\Omega}_e \right] \cdot \cos\beta_0 + \left( y_n \Omega_e \Omega_\beta - \frac{1}{2} x_n \dot{\Omega}_\beta \right) \cdot \sin\beta_0 \right\}$$

$$R'''_\Omega = -\left[ \frac{1}{2} y_n \cos\beta_0 \Omega_e \Omega_\beta^2 + \frac{1}{2} (x_n \Omega_e^2 \Omega_\beta - y_n \dot{\Omega}_e \Omega_\beta + y_n \Omega_e \dot{\Omega}_\beta) \sin\beta_0 \right]$$

$$s(f, t_m) = \sum_n A_n \exp[-j \frac{4\pi}{c} (f_c + f_r) (R_\Omega + R'_\Omega t_m + R''_\Omega t_m^2 + R'''_\Omega t_m^3)]$$

the remainder of this section is evaluating the varyaction the bistatic angle and composite LOS angle in receiver centered region. Bistatic system operation at L band and bandwidth is 400 MHz, baseline is 100Km.

## Super resolution algorithm in receiver cantered region

In this section, we will propose new algorithm aim at estimating instantaneous Doppler, chirp rate and quadchirp rate spectrum of signal components which suitable for generating high resolution ISAR image in receiver centered region. The algorithm usesrandon transforming TCD of echoes and employing the Relax searching iterative procedure which has excellent performance of global optimum parameter estimating in super resolution ISAR imaging. TCD was studied and described by O'Neill [8-10]. It is suitable for the estimation of the instantaneous chirp rate spectrum. A quadratic frequency modulated signal has the following form

$$\begin{aligned} s(t) &= \exp[j\Phi(t)] \\ &= \exp\left[ j\left( \Phi_0 + f \cdot t + \frac{1}{2}\mu \cdot t^2 + \frac{1}{6}\dot{\mu} \cdot t^3 \right) \right] \end{aligned}$$

where Φ0 is the initial phase, and f is the initial freequench, μ is defined as the chirp rate and $\dot{\mu}$ is the change rate of chirp, called the quadratic chirp rate. The timechirp distribution of (25) can be written as

$$\begin{aligned} TCD_s(t, c) &= \int Z_s(t, \tau) \exp(-jc\tau) d\tau \\ &= \int \exp\left\{ -j\tau \left[ c - \dot{\mu}(t) \right] \right\} d\tau \\ &= 2\pi\delta\left[ c - \dot{\mu}(t) \right] \end{aligned}$$

$$Z_s(t, \tau) = \begin{cases} s(t + \sqrt{\tau}) s^*(t) s^*(t) s(t - \sqrt{\tau}), & \tau \geq 0 \\ Z_s^*(t, -\tau), & \tau < 0 \end{cases}$$

Where

$$\mu(t) = \mu + \dot{\mu} \cdot t$$

ISSN: 1000-372X ALT

is the delta function, and represents the current chirp rate at any given moment? Linear instantaneous chirp rate (t) seems to be where the TCD of a QFM signal is concentrated. The chirp rate and quadrupole chirp rate may be estimated by taking the Radon transform of the signal in the TCD plane and finding its peak location. When there are numerous signals present at once, interference cross-terms also appear in the TCD plane. To avoid practical difficulties caused by cross terms, it is necessary to integrate the signal energy in the same manner as the Radon-Wigner transform [11]. Figure 4 depicts a single-component QFM signal and the resulting Radon transform to demonstrate the TCD of a QFM signal. After doing the aforesaid study, we suggest a new approach that is well suited to imaging a moving object in the receiver-centered area, where the target's signal is in the QFM forms. That is the Relax algorithm for the Radon time chirp distribution. We proposed concentrating the strategies on estimating the general cross range phase parameter after translation motion correction had been applied, using range cell alignment and phase autofocus. We refer to this method as the Radon-TCDS-Relax algorithm.

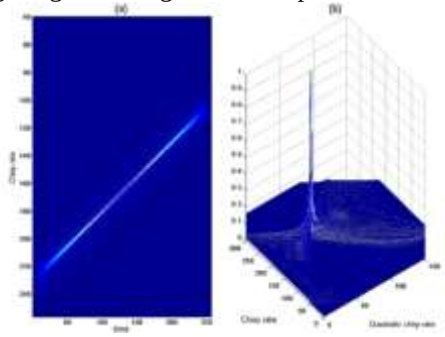

*figure 4 QFM time-chirp distribution and Radon transform (a) equ.25 time-chirp distribution. (b) (a) Radon transform result.*

For an arbitrary range cell, the signal of target can be modelled as a sequence s(n) that consists of K complex QFM signal in the presence of AR noise [12-14].

$$s(n)=\sum_{k=1}^{K}\alpha_k \exp\left(j2\pi f_k n+j\pi\mu_k n^2+\frac{1}{3}j\pi\ \dot{\mu}_k n^3\right)+e(n)$$

where n = 0, 1, ⋯ N − 1, N is the sample number in slow time, e(n) is AR noise. As we know, the parametric relaxation based algorhythm suitable for estimation the complex amplitude and sinusoidal frequency. For expanding Relax to chirp signal model, let

$$\mathbf{y}=[y(0)\quad y(1)\quad\cdots\quad y(N-1)]^T$$

And

$$\psi_k=\left[1\quad \exp\left(j2\pi f_k+j\pi\mu_k+\frac{1}{3}j\pi\ \dot{\mu}_k\right)\quad\cdots\quad \exp\left(j2\pi f_k(N-1)+j\pi\mu_k(N-1)^2\right)+\frac{1}{3}j\pi\ \dot{\mu}_k(N-1)^3\right]^T$$

where [·] T . The parameters αk

$$\left\{\alpha_k, f_k, \mu_k,\ \dot{\mu}_k\right\}(k=1,2\cdots K)$$

can be estimation via minimizing the follwongno linear least squares (NLS) criterion.

$$C_1\left(\left\{\alpha_k, f_k, \mu_k,\ \dot{\mu}_k\right\}_{k=1}^{K}\right)=\left\|\mathbf{y}-\sum_{k=1}^{K}\alpha_k\psi_k\right\|^2$$

## Simulation result

Figure 5 depicts a bistatic radar system's transmitter and receiver. The target is located 100 kilometres from the transmitter and 6 kilometres from the receiver; the baseline length, L, is 100 kilometers. In this section's last subsection, we'll calculate the shift in bistatic angle and composite LOS angle in the area cantered on the receiver. L-band radar with a bandwidth of 400 MHz and a baseline of 100 kilometres. Target's x-axis velocity is v=400m/s, and the distance between the target and the radar receiver is 6 kilometres. An L-band radar uses a frequency of 1200 MHz as its carrier and a transmission bandwidth of 400 MHz Rt = 100Km, RR = 6Km are the starting values for the distance between the transmitter and receiver. R = 90°, T = 3.43° are the line-of-sight angles between the transmitter and receiver. e = 46.78 is the corresponding monostatic LOS angle. Coherent integra tion takes place over the course of 3 seconds when the initial biostatic angle is = 43.28 and the wavelength is = 0.03m. There are 330-point scatterers that make up the virtual plane. Figure 6a depicts the plane's model, and its dimensions.

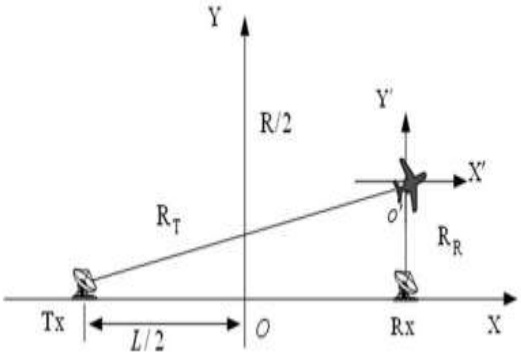


***Figure 5 The plane and Biostatic model geometry***

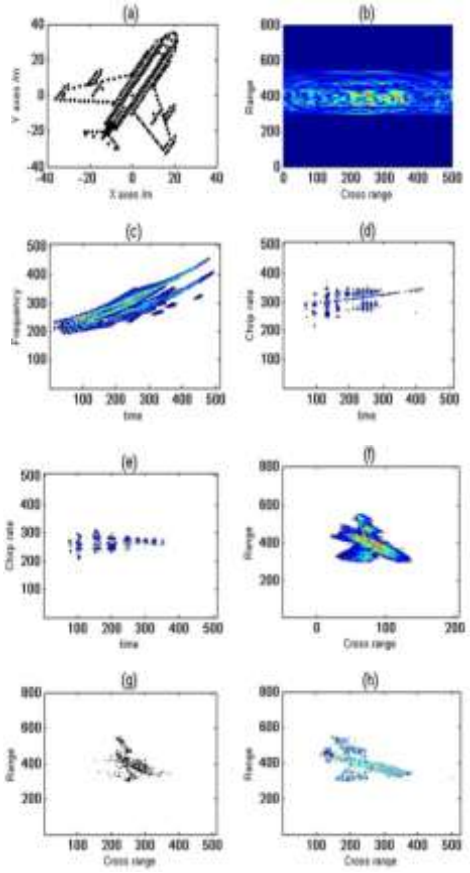


***Figure 6 Simulation results (a) Yikker 42 model. (b) envelope after alignment. (c) time frequency distribution. (d) t-cd distribution of range cell before quadratic chirp rate correction. (e) t-cd distribution of range cell before quadratic chirp rate correction (f) RD imaging result. (g) Dechirpclean imaging result. (h) Radon-TCDS-Relax imaging result.***

is around 80 meters on each side. Let's pretend the conventional has done away with the MTRC phenomena. Third-order phasor term migration between ranges has to be taken into account. Figure 6b depicts the envelope

ISSN: 1000-372X ALT

of echo after it has been keystone-formatted and translational motion-compensated. The alignment of the envelope is visible. The frequency and chirp distributions of the signal over time in a single range cell are shown in Figure 6c and 6d, respectively. The presence of the cubic phase term causes the data to have a curved distribution in the time-frequency plane and a linear distribution in the time chirp plane. After the quad ratic chirp rate estimated and compensated the cubic phase term, as shown in Figure 6e, the data exhibit a linear distribution in the time -chirp plane, spreading out along a beeline perpendicular to the time axis. Based on Figure 6f, we can see that the RD imaging result is flawed since the third order component in phase has not been adequately adjusted, therefore we can only make out the target's general shape but not any of its finer features. Image 6g displays the outcome of the Decicycle imaging process. The upper tail and wing of the fuselage are obscured because third order terms are not eliminated adequately. In Figure 6h, the imaging result from Radon-TCDS-Relax, we can see that the model features are represented rather well. The chirp rate and frequency have been calculated with high precision. The efficacy of the suggested technique has been verified, and the ISAR picture contains very few false scatterers.

## Conclusions

The range envelope and cross range in a bistatic ISAR system are sensitive to changes in bistatic angle and corresponding monostatic angel in the receiver-cantered area. The high-order phase term must be taken into account. To acquire a high-resolution picture of the target, this study proposes a novel ISAR imaging technique called Radon-TCDS-Relax for the bistatic receiver's central area, which estimates the chirp rate and a quadratic chirp rate in the time chirp distribution plane. The simulation result demonstrates that the suggested approach outperforms the traditional RD and RID ISAR imaging methods in terms of picture quality, and the efficacy of the new algorithm is also confirmed.

## References

***[1]. CC Chen, HC Andrews, Target-Motion-Induced Radar Imaging. IEEE Trans on AES 16(1), 2–14 (1980)***

***[2]. JP Marco Martorell, H John, Ambiguity Function for a Bistatic Radar. IEEE Transactions on AES 43(3), 1125–1134 (2007)***

***[3]. J Palmer, J Homer, ID Longstaff et al., ISAR imaging using an emulated multistatic radar system. IEEE Transactions on AES 41(4), 1464–1472 (2005)***

***[4]. T Tsao, M Slamani, P Varshney et al., Ambiguity Function for a Bistatic Radar. IEEE Transactions on AES 33(3), 1041–1051 (1997)***

***[5]. MI Skolnik, Radar Handbook[M] (McGraw-Hill, Inc, 1970)***

***[6]. M Xing, Z Bao, Imaging algorithm for steadily flying and maneuvering big targets. Proc. SPIE 4382, 182–190***

ISSN: 1000-372X ALT